

Crossed-beam reaction of carbon atoms with hydrocarbon molecules. II. Chemical dynamics of $n\text{-C}_4\text{H}_3$ formation from reaction of $\text{C}(^3P_j)$ with methylacetylene, $\text{CH}_3\text{CCH}(X^1A_1)$

R. I. Kaiser, D. Stranges,^{a)} Y. T. Lee,^{b)} and A. G. Suits^{c)}

Department of Chemistry, University of California, Berkeley, California 94720
and Chemical Sciences Division, Berkeley National Laboratory, Berkeley, California 94720

(Received 28 June 1996; accepted 9 July 1996)

The reaction between ground-state carbon atoms, $\text{C}(^3P_j)$, and methylacetylene, $\text{CH}_3\text{CCH}(X^1A_1)$, was studied at average collision energies of 20.4 and 33.2 kJ mol^{-1} using the crossed molecular beams technique. Product angular distributions and time-of-flight spectra of C_4H_3 at $m/e=51$ were recorded. Forward-convolution fitting of the data yields weakly polarized center-of-mass angular flux distributions isotropic at lower, but forward scattered with respect to the carbon beam at a higher collision energy. The translational energy flux distributions peak at 30–60 kJ mol^{-1} and show an average fractional translational energy release of 22%–30%. The maximum energy release as well as the angular distributions are consistent with the formation of the $n\text{-C}_4\text{H}_3$ radical in its electronic ground state. Reaction dynamics inferred from these distributions indicate that the carbon atom attacks the π -orbitals of the methylacetylene molecule via a loose, reactant like transition state located at the centrifugal barrier. The initially formed triplet 1-methylpropendiyldiene complex rotates in a plane almost perpendicular to the total angular momentum vector around the $B\backslash C$ -axes and undergoes [2,3]-hydrogen migration to triplet 1-methylpropargylene. Within 1–2 ps, the complex decomposes via C–H bond cleavage to $n\text{-C}_4\text{H}_3$ and atomic hydrogen. The exit transition state is found to be tight and located at least 30–60 kJ mol^{-1} above the products. The explicit identification of the $n\text{-C}_4\text{H}_3$ radical under single collision conditions represents a further example of a carbon–hydrogen exchange in reactions of ground state carbon atoms with unsaturated hydrocarbons. This channel opens a versatile pathway to synthesize extremely reactive hydrocarbon radicals relevant to combustion processes as well as interstellar chemistry. © 1996 American Institute of Physics. [S0021-9606(96)00739-8]

I. INTRODUCTION

The interstellar medium (ISM) consists of gas and sub μm sized grain particles with averaged number densities of 1 H atom cm^{-3} and 10^{-11} grains cm^{-3} . Its chemical composition is dominated by hydrogen and helium (H:He \approx 1:0.1), whereas the biogenic elements oxygen, carbon, and nitrogen contribute \approx 0.001 relative to atomic hydrogen.^{1–2} Comprising approximately 99% neutrals and 1% ions, interstellar radicals, atoms, and molecules are not distributed homogeneously, but primarily localized in interstellar clouds as well as outflow of carbon stars.^{1–2} Diffuse (hot) clouds hold number densities n up to 100 molecules cm^{-3} and mean translational temperatures T of about 100 K, whereas in dense (cold, dark, molecular) clouds typical scenarios range between $n=10^2\text{--}10^6$ cm^{-3} and $T=10\text{--}40$ K. Molecules in the outflow of carbon stars contribute only a minor amount, but temperatures can rise up to 4000 K,³ and a more complex chemistry is expected as compared to interstellar clouds.

Since the average kinetic energy of the interstellar species is confined to typically 0.8 kJ mol^{-1} (diffuse clouds) and

0.08 kJ mol^{-1} (dark clouds), gas phase reactions under thermodynamic equilibrium conditions must have little or no barriers and involve only two body collisions. Ternary encounters occur only once in a few 10^9 years, and can be excluded considering mean interstellar cloud lifetimes of 10^6 years.⁴ The first chemical equilibrium models of interstellar chemistry satisfy these criteria and focus on ion-molecule reactions, radiative associations, as well as dissociative recombination between cations and electrons to advance interstellar chemistry.^{5,6} This approach, however, involves reaction chains with subsequent collisions, and often cannot reproduce observed structural isomer ratios as well as number densities for example of C_3H and C_3H_2 .⁷ The inclusion of alternative, one step, exothermic neutral–neutral reactions into chemical models of the circumstellar envelope surrounding the carbon star IRC+10216 and the dark cloud TMC-1 occurred only gradually.^{8–16} However, the *ad hoc* postulation of spin conservation and simple thermochemistry clearly demonstrate the urgency of systematic laboratory examinations probing detailed chemical dynamics and reaction products of neutral–neutral encounters.

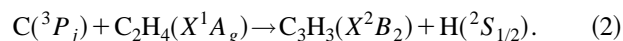
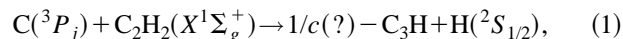
Very recently, these studies were initiated investigating exothermic atom-molecule reactions of atomic carbon in its 3P_j electronic ground state with unsaturated hydrocarbons

^{a)}Present address: Dipartimento Chimica, Universita La Sapienza, Piazzale A. Moro 5, 00185 Rome, Italy.

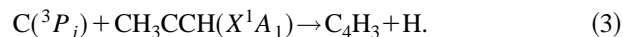
^{b)}Present address: Academia Sinica, Nankang, Taipei, 11529, Taiwan.

^{c)}Author to whom correspondence should be addressed.

via the crossed beam technique as a potential source of carbon hydride and the propargyl radical^{7,17}



The explicit identification of this carbon–hydrogen exchange channel opens a versatile synthetic pathway to carbon bearing species. Analogous to Eq. (1), reaction of $\text{C}(^3P_j)$ with methylacetylene, CH_3CCH , is expected to yield hitherto unobserved interstellar C_4H_3 isomer(s)

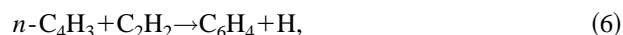
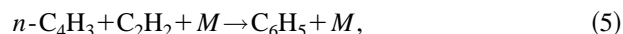


Its prospective methylacetylene precursor and atomic carbon have been widely observed in the molecular clouds OMC-1¹⁸ and TMC-1¹⁹ with fractional abundances relative to hydrogen between 4×10^{-9} and 6.3×10^{-9} . Likewise, methylacetylene^{20–22} as well as C_4H_3 isomers are included in a photochemical model of Titan, Jupiter, and Saturn.^{23–24} The authors postulate C_4H_3 formation via three body recombination



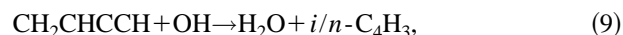
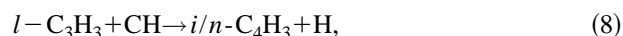
although cosmic ray produced carbon atoms survive the reducing atmospheres²⁵ and might react via Eq. (3).

Besides its potential interstellar relevance, a scavenged C_4H_3 isomer in acetylene/oxygen flames²⁶ is expected to play a significant role in formation of the first aromatic ring in sooting combustion flames. Wang *et al.* postulated a stepwise ring growth initiated by Eq. (5) or (6) to the phenyl radical or benzyne²⁷

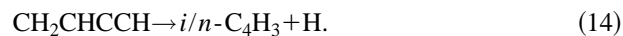


whereas Walsh outlined *i*- C_4H_3 reacts with only a minor entrance barrier as well.²⁸

However, no reliable information is available on the mechanism of C_4H_3 radical formation. Miller *et al.* suggested pathways via Eqs. (7)–(10),²⁹ followed by interconversion of *i/n*- C_4H_3 [Eq. (11)]



Alternatively, acetylene dimerization [Eq. (12)],^{30–31} recombination with C_2H [Eq. (13)],³² and thermal decomposition of vinylacetylene intermediates [Eq. (14)]^{33–35} might yield C_4H_3



Although atomic carbon is only a minor species in oxidative flames, it is assumed to contribute significantly to combustion chemistry,³⁶ and the carbon–hydrogen exchange channel [Eq. (3)] could synthesize several C_4H_3 isomers as well as advance diamond synthesis in methylacetylene flames.³⁷

However, despite the potential astrochemical and combustion relevance, the experimental as well as theoretical characterization of the C_4H_3 PES is far from being complete, Fig. 1. *n*- C_4H_3 (1*a/b*) holds the global minimum on the doublet C_4H_3 PES ($\Delta_f H = 486 \pm 3$ kJmol⁻¹),^{28,38–39} followed by a 40 ± 1 kJmol⁻¹ less stable iso isomer (2) ($\Delta_f H = 526 \pm 4$ kJmol⁻¹).^{28,38} The structure of *n*- C_4H_3 has not yet been resolved. Gay *et al.* calculated a bent, α -ethinylvinyl carbon skeleton, whereas ESR studies in an argon matrix at 4 K support a linear structure with 2B_2 electronic ground state of the butatrienyl radical.^{40–41} Very recently, high level *ab initio* calculations at the SCF-CISD(6-311G**) level depict a quasilinear structure (1*a*) and an interconversion barrier between both bent C_4H_3 conformations (1*b*) of only 3 kJmol⁻¹.⁴² Since the C_4H_3 isomers are extremely reactive, isolation is restricted to a low temperature matrix (*n*- C_4H_3) or trapping as an 1,3- μ_3 -dimetalated cyclic species (*M1*) as well as 1,3,3- μ_4 -trimetalated chain isomer (*M2*).^{43–44}

In this paper, we investigate the detailed chemical dynamics of the atom-neutral reaction of $\text{C}(^3P_j)$ with methylacetylene, $\text{CH}_3\text{CCH}(X^1A_1)$ under single collision conditions at collision energies of 20.4 and 33.2 kJmol⁻¹ as provided in crossed molecular beam experiments. The insights into the reaction dynamics disclose precise information on the hitherto unexplored triplet C_4H_4 and doublet C_4H_3 potential energy surface (PES) under well-defined collision energies, and potential exit channel(s) to C_4H_3 isomers.

II. EXPERIMENTAL SETUP AND DATA ANALYSIS

Owing to the high reactivity of prospective open shell products, reactions must be performed under single collision conditions to identify the primary reaction products. These requirements are achieved here using a universal crossed molecular beam apparatus described in Ref. 45 in detail. A pulsed supersonic carbon beam was generated via laser ablation of graphite at 266 nm.⁴⁶ The 30 Hz, 35–40 mJ output of a Spectra Physics GCR-270-30 Nd:YAG laser is focused onto a rotating carbon rod. Ablated carbon atoms are seeded into neon or helium released by a Proch–Trickl pulsed valve operating at 60 Hz, 80 μs pulses, and 4 atm backing pressure. A four slot chopper wheel mounted 40 mm after the ablation zone selects a 9.0 μs segment of the seeded carbon beam. Table I compiles the experimental beam conditions. The pulsed carbon and a continuous methylacetylene beam at 515 ± 10 Torr backing pressure pass through skimmers, and cross at 90° in the interaction region of the scattering

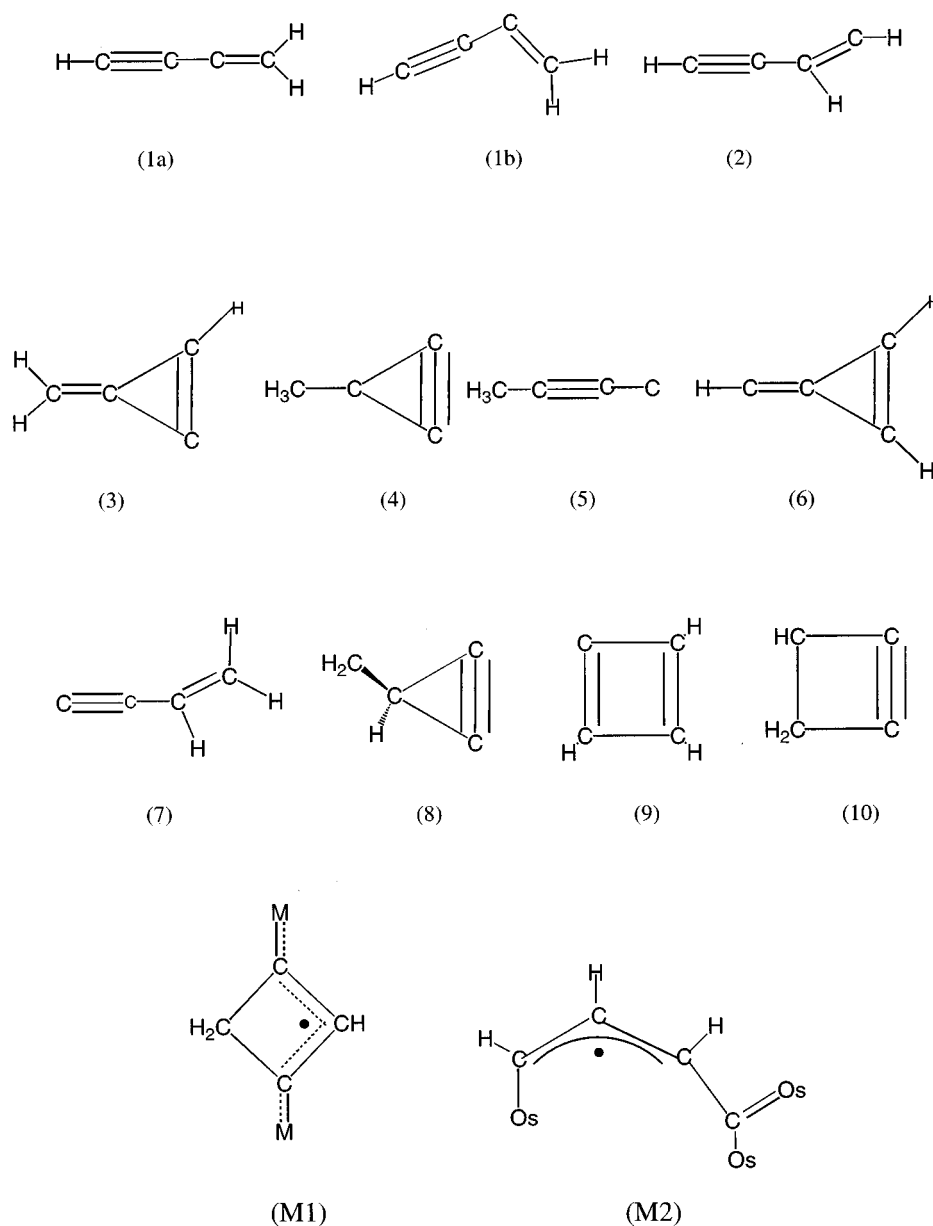


FIG. 1. Structures of low lying C_4H_3 isomers as well as metalated radicals M1 and M2. A linear isomer of Eq. (4), analogous to the $c/1-C_3H$ isomer pair, has not been investigated. Since $c-$ and $1-C_3H$ differ only by $8 \pm 4 \text{ kJmol}^{-1}$, the linear isomer (5) holds approximately $\Delta_f H = 560 \text{ kJmol}^{-1}$. Other enthalpies of formations for the isomers are (1) 486, (2) 526, (3) 541, (4) 553, (6) 572, (7) 604, (8) 613, (9) 660, and (10) 766 kJmol^{-1} .

chamber. Reactively scattered products were detected in the plane of the beams using a rotatable detector consisting of a Brink-type electron-impact ionizer,⁴⁷ quadrupole mass filter, and a Daly ion detector⁴⁸ at different laboratory angles in

5.0° steps between 5.0° and 60.0° with respect to the carbon beam. The velocity distribution of the products was recorded using the time-of-flight (TOF) technique⁴⁹ choosing a channel width of $7.5 \mu\text{s}$. Counting times ranged from $0.5\text{--}4 \text{ h}$,

TABLE I. Experimental beam conditions and 1σ errors averaged over the experimental time: Most probable velocity v_0 , speed ratio S , most probable relative collision energy, E_{coll} , center-of-mass angle, θ_{CM} , composition of the carbon beam, and flux factor $f_v = n(\text{C}) \times n(\text{C}_3\text{H}_4) \times v_r$, in relative units, with the number density of the i th reactant n_i and the relative velocity v_r .

Beam	v_0, ms^{-1}	S	$E_{\text{coll}}, \text{kJ mol}^{-1}$	θ_{CM}	$C_1:C_2:C_3$	f_v
$C(^3P_j)/\text{Ne}$	1950 ± 40	3.9 ± 0.3	20.4 ± 1.0	53.5 ± 1.5	1:0.6:0.7	1.0
$C(^3P_j)/\text{He}$	2560 ± 50	4.7 ± 0.3	33.2 ± 1.4	46.2 ± 1.6	1:0.4:0.9	1.8 ± 0.3
C_3H_4	790 ± 30	7.7 ± 0.5

averaged over several angular scans. The velocity of the supersonic carbon beam was monitored frequently after 2–5 angles and minor velocity drifts corrected by adjusting the laser pulse delay within $\pm 1.5 \mu\text{s}$. A reference angle was chosen at 55° and 45° , respectively, to calibrate fluctuating carbon beam intensities and mass dial settings at the quadrupole controller.

Information on the reaction dynamics is gained by fitting the TOF spectra and the product angular distribution in the laboratory frame using a forward-convolution routine.^{50–51} This iterative approach initially guesses the angular flux distribution $T(\theta)$ and the translational energy flux distribution $P(E_T)$ in the center-of-mass system (CM) assuming mutual independence. Laboratory TOF spectra and the laboratory angular distributions were then calculated from these $T(\theta)$ and $P(E_T)$ averaged over a grid of Newton diagrams defining the velocity and angular spread of each beam, detector acceptance angle, and the ionizer length. Best TOF and labo-

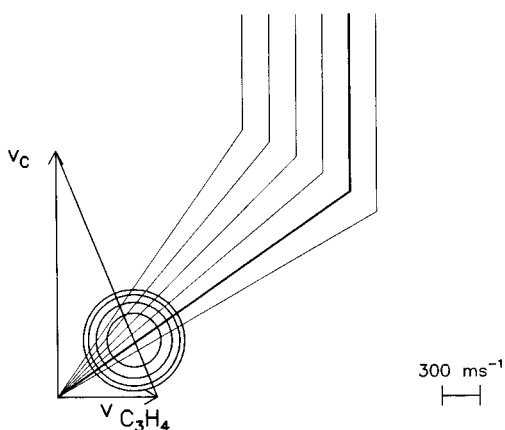
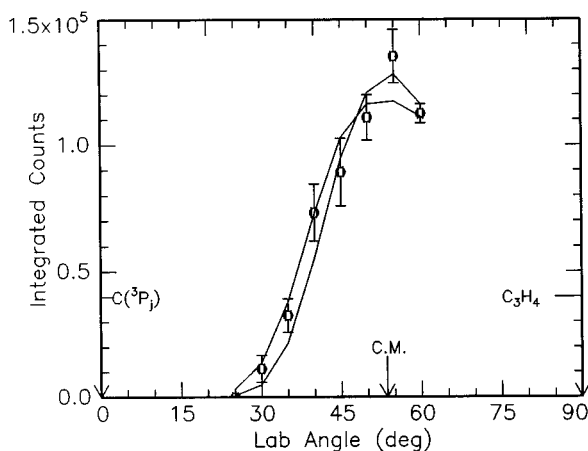


FIG. 2. Lower: Newton diagram for the reaction $\text{C}(^3P_j) + \text{CH}_3\text{CCH}(X^1A_1)$ at a collision energy of 20.4 kJmol^{-1} . The circles stand for the maximum center-of-mass recoil velocity. From outer to inner: *n*- C_4H_3 , *i*- C_4H_3 , C_4H_3 isomers (3)–(8), and C_4H_3 isomer (9). Upper: Laboratory angular distribution of product channel at $m/e=51$. Circles and 1σ error bars indicate experimental data, the solid lines the calculated distribution for the upper and lower carbon beam velocity (Table I). C.M. designates the center-of-mass angle. The solid lines originating in the Newton diagram point to distinct laboratory angles whose TOFs are shown in Fig. 4.

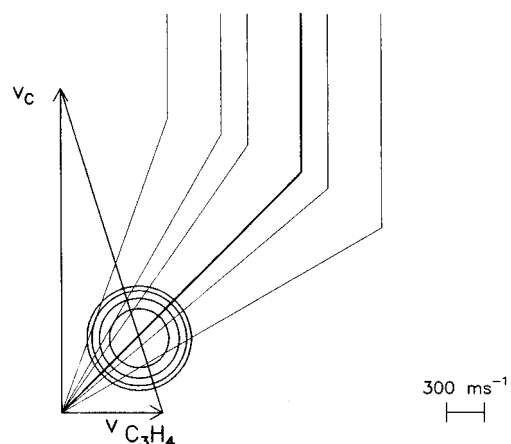
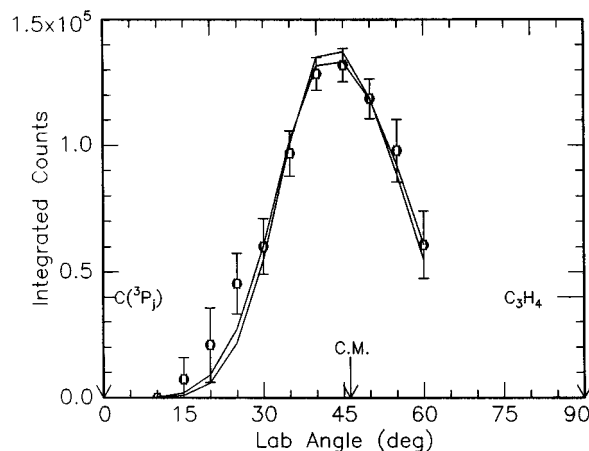


FIG. 3. Lower: Newton diagram for the reaction $\text{C}(^3P_j) + \text{CH}_3\text{CCH}(X^1A_1)$ at a collision energy of 33.2 kJmol^{-1} . The circles are corrected for difference in the relative collision energy. Upper: Laboratory angular distribution of product channel at $m/e=51$. Circles and 1σ error bars indicate experimental data, the solid lines the calculated distribution for the upper and lower carbon beam velocity. The solid lines originating in the Newton diagram point to distinct laboratory angles whose TOFs are shown in Fig. 5.

ratory angular distributions were archived by iteratively refining adjustable $T(\theta)$ and $P(E_T)$ parameters.

III. RESULTS

A. Reactive scattering signal

Reactive scattering signal was only observed at $m/e=51$, i.e., C_4H_3 , cf. Figs. 2–5 and Table II. Reaction of carbon with methylacetylene dimers does not contribute the data, since the integrated $m/e=51$ signal scales linearly with the CH_3CCH source backing pressure. TOF spectra recorded at $m/e=48$ – 50 show identical patterns indicating the signal originates in cracking of the parent in the detector. Energetically accessible channels 2 and 3 to diacetylene (Table II), C_4H_2 , are absent within detection limits of our system, and endothermic channels 3 and 4 could not be opened at relative collision energies up to 33.2 kJmol^{-1} applied in our experiments. In addition, no radiative association to C_4H_4 isomers at $m/e=52$ or higher masses were observed. Lower molecular weight products bearing two or three carbon atoms (exo-

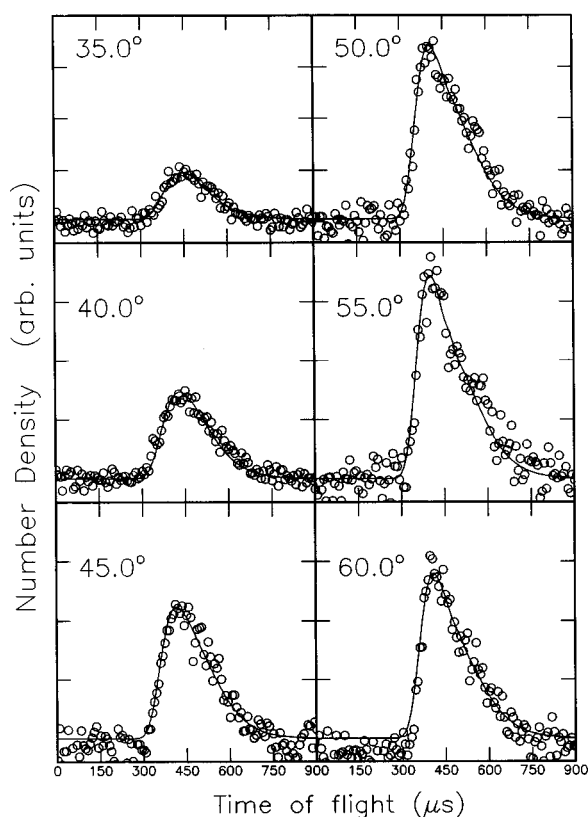


FIG. 4. Time-of-flight data at $m/e=51$ for indicated laboratory angles at a collision energy of 20.4 kJmol^{-1} . Open circles represent experimental data, the solid line the fit. TOF spectra have been normalized to the relative intensity at each angle.

thermic channels 6–12) could not be verified yet. Their detection suffers from the high background level via methylacetylene fragmentation in the ionizer. Upper limits of 40% (channels 6–8), 60% (channel 9), 10% (channel 10), 40% (channels 11), and 80% (channel 12) relative to $m/e=51$ signal were derived.

B. Laboratory angular distributions (LAB) and TOF spectra

Figures 2 and 3 display the most probable Newton diagrams of the title reaction as well as the laboratory angular (LAB) distributions of the C_4H_3 product at collision energies of 20.4 and 33.2 kJmol^{-1} , respectively. Both LAB distributions peak close to the CM angles at 53.5° and 46.2° and show a slightly forward peaking distribution at higher collision energy. This behavior suggests indirect reaction dynamics via a long-lived C_4H_4 complex with a lifetime exceeding (20.4 kJmol^{-1}) or comparable to its rotational period (33.2 kJmol^{-1} , osculating complex). Since the enthalpy of formation of low lying C_4H_3 isomers differs only by about $30\text{--}50 \text{ kJmol}^{-1}$, Fig. 1, the nature of the C_4H_3 solely based on limiting circles is not possible. The maximum scattering range of isomers (1)–(8) falls within 8° , and individual limit circles are blurred out due to the velocity spread of the carbon beam (Table I). However, the scattering range of the $m/e=51$

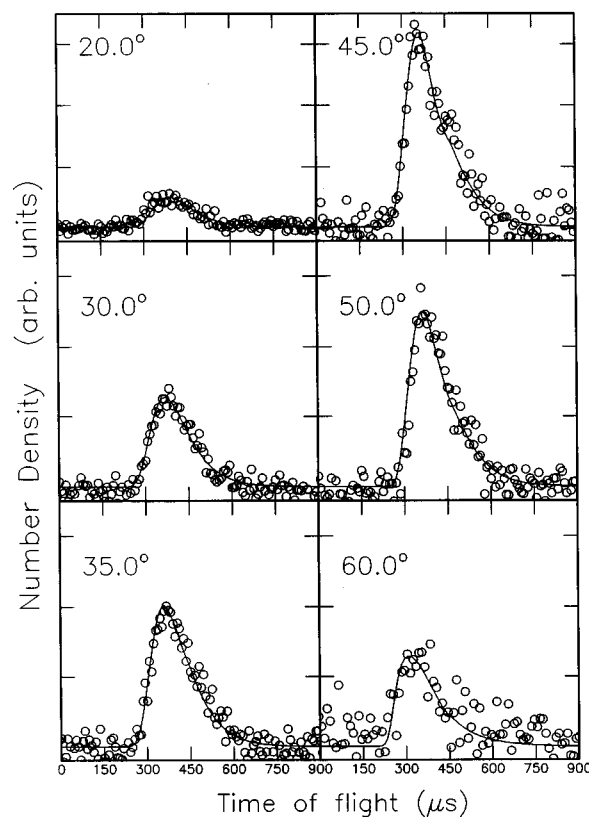


FIG. 5. Time-of-flight data at $m/e=51$ for indicated laboratory angles at a collision energy of 33.2 kJmol^{-1} . Open circles represent experimental data, the solid line the fit. TOF spectra have been normalized to the relative intensity at each angle.

product allows us to eliminate isomer (9) and the endothermic channel to isomer (10). Further, the large width of the laboratory angular distribution of at least 60° and the $\text{C}_4\text{H}_3+\text{H}$ product mass ratio of 51 indicates that the average translational energy release $\langle E_T \rangle$ is large and that the center-of-mass translational energy distributions $P(E_T)s$ peak well away from zero, cf. Sec. III C.

TABLE II. Thermochemistry of the reaction $\text{C}(^3P_j)+\text{CH}_3\text{CCH}(X^1A_1)$. Enthalpies of formations were taken from Refs. 28, 38, 39, 52, and 53. The symmetry of the $n\text{-C}_4\text{H}_3$ ground-state electronic wave function is omitted.

#	Exit channel	Reaction enthalpy at 0 K, $\Delta_R H$ (0 K), kJ mol^{-1}
1	$n\text{-C}_4\text{H}_3(?) + \text{H}(^2S_{1/2})$	-194 ± 1
2	$\text{HCCCCH}(X^1\Sigma_g^+) + \text{H}_2(X^1\Sigma_g^+)$	-444 ± 12
3	$\text{HCCCCH}(X^1\Sigma_g^+) + 2\text{H}(^2S_{1/2})$	-12 ± 12
3	$\text{C}_4\text{H}(X^2\Sigma) + \text{H}_2(X^1\Sigma_g^+) + \text{H}(^2S_{1/2})$	$+78 \pm 10$
4	$\text{C}_4(X^3\Sigma_g^-) + 2\text{H}_2(X^1\Sigma_g^+)$	$+68 \pm 15$
5	$\text{C}_3\text{H}_3(X^2B_2) + \text{CH}(X^2\Pi)$	$+35 \pm 12$
6	$c\text{-C}_3\text{H}_2(X^1A_1) + \text{CH}_2(X^3B_2)$	-22 ± 5
7	$c\text{-C}_3\text{H}(X^2B_2) + \text{CH}_3(X^2A_2')$	-36 ± 4
8	$l\text{-C}_3\text{H}(X^2\Pi) + \text{CH}_3(X^2A_2')$	-28 ± 4
9	$\text{C}_3(X^1\Sigma_g^+) + \text{CH}_4(X^1A_1)$	-151.5 ± 1
10	$\text{C}_2\text{H}_4(X^1A_g) + \text{C}_2(X^1\Sigma_g^+)$	-6 ± 1
11	$\text{C}_2\text{H}_3(X^2A') + \text{C}_2\text{H}(X^2\Sigma^+)$	-30 ± 6
12	$\text{C}_2\text{H}_2(X^1\Sigma_g^+) + \text{C}_2\text{H}_2(X^1\Sigma_g^+)$	-440 ± 1

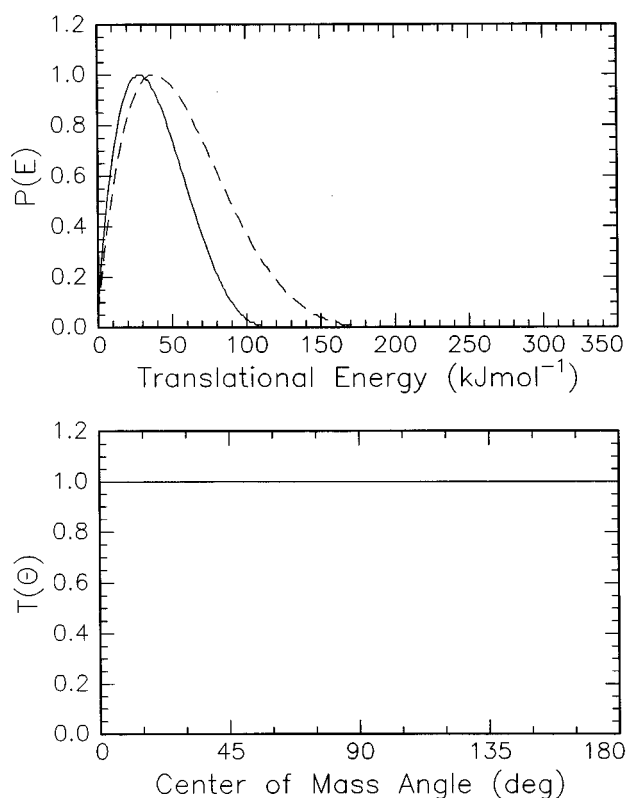


FIG. 6. Lower: Center-of-mass angular flux distribution for the reaction $C(^3P_j)+CH_3CCH(X^1A_1)$ at a collision energy of 20.4 kJmol^{-1} . Upper: Center-of-mass translational energy flux distribution for the reaction $C(^3P_j)+CH_3CCH(X^1A_1)$ at a collision energy of 20.4 kJmol^{-1} . Dashed and solid lines limit the range of acceptable fits within 1σ error bars.

C. Center-of-mass translational energy distributions, $P(E_T)$

Figures 6 and 7 present the translational energy distributions $P(E_T)$ and angular distributions $T(\theta)$ in the center-of-mass frame. Both LAB distributions and TOF data were fitted with a single $P(E_T)$ extending to a maximum translational energy release E_{\max} of $110\text{--}170 \text{ kJmol}^{-1}$ and $225\text{--}255 \text{ kJmol}^{-1}$, respectively. If the energetics of distinct isomers are well separated, E_{\max} can be used to identify individual C_4H_3 isomers. The maximal translational energy releases, i.e., the sum of the reaction exothermicity and relative collision energy, were already presented in Figs. 2 and 3 with a reasonable approximation of rotationally and vibrationally cold methylacetylene molecules prepared in the supersonic expansion. The production of the $n-C_4H_3$ isomer at 33.2 kJmol^{-1} is evident by comparing the theoretical and experimental high energy cutoff of $P(E_T)$ with $E_{\max}(\text{exp.}; 33.2 \text{ kJmol}^{-1})=225\text{--}255 \text{ kJmol}^{-1}$ vs $E_{\max}(\text{theor.}; 33.2 \text{ kJmol}^{-1})=226\pm 7 \text{ kJmol}^{-1}$. Formation of the 40 kJmol^{-1} less stable iso isomer can be rejected, since the maximum energy release is restricted to 186 kJmol^{-1} . Based entirely on the high energy cutoff, the reactive scattering product at lower collision energy is hard to identify, since all C_4H_3

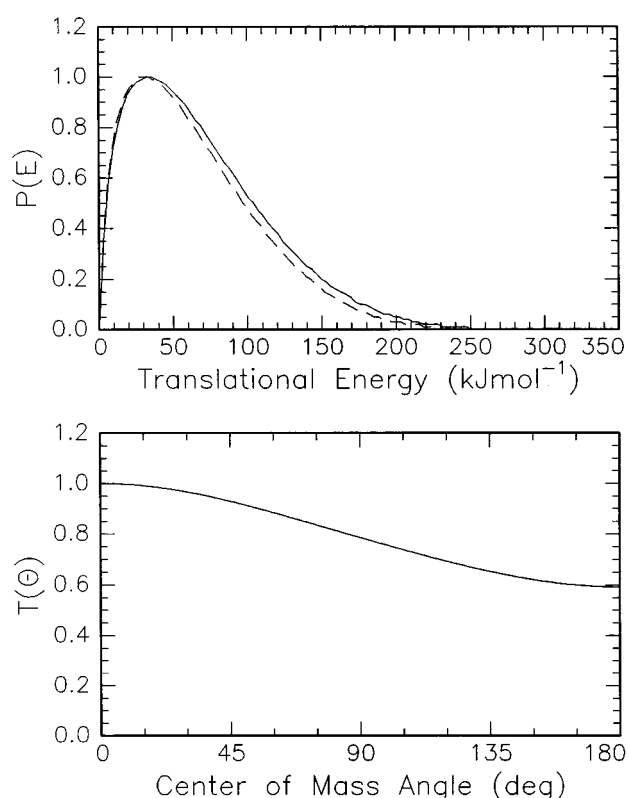


FIG. 7. Lower: Center-of-mass angular flux distribution for the reaction $C(^3P_j)+CH_3CCH(X^1A_1)$ at a collision energy of 33.2 kJmol^{-1} . Upper: Center-of-mass translational energy flux distribution for the reaction $C(^3P_j)+CH_3CCH(X^1A_1)$ at a collision energy of 33.2 kJmol^{-1} . Dashed and solid lines limit the range of acceptable fits within 1σ error bars.

isomers (2)–(6) fall within the E_{\max} range. Due to the internal excitation of the C_4H_3 product, even Eq. (1) cannot be ruled out, cf. Sec. III D.

Besides identification of structural isomers, the most probable translational energy yields the order-of-magnitude of the barrier height in the exit channel. Both $P(E_T)$ s peak away from zero as expected from the LAB distributions and depict a broad plateau between $30\text{--}60 \text{ kJmol}^{-1}$. A exit barrier is further implied by the large fraction of energy channeled into translational motion of the C_4H_3 and H products, i.e., $22\pm 5\%$ and $30\pm 3\%$ at lower and higher collision energy, respectively. These findings suggest a tight transition state with a significant change in electronic structure as the C_4H_4 complex decomposes.

D. Center-of-mass angular distributions, $T(\theta)$

At lower collision energy, $T(\theta)$ is isotropic and symmetric around $\pi/2$ implying that either the fragmenting C_4H_4 holds a lifetime longer than its rotational period τ_r or that the exit transition state is symmetric.^{54–55} With increasing collision energy, the center-of-mass angular distribution peaks forward with respect to the carbon beam. These findings indicate a reduced lifetime of the decomposing C_4H_4 complex and agrees with our suggested osculating complex: a com-

plex formation takes place, but the well depth along the reaction coordinate is too shallow to allow multiple rotations, and the complex decomposes with a random lifetime distribution before one full rotation elapses. Based on the intensity ratio of $T(\theta)$ at $\theta=0^\circ$ and 180° of 1.7 ± 0.1 , the identification of the fragmenting complex enables us to use the rotational period of the complex as a molecular clock to estimate its lifetime (cf. Sec. IV D). To explain the forward-peaking, the carbon atom and the leaving hydrogen atom must further be situated on opposite sites of the rotation axis of the fragmenting complex.

The weak polarization of all $T(\theta)$ s can be explained solely based on total angular momentum conservation and angular momentum disposal.^{17,54,55} In terms of a classical treatment, the total angular momentum \mathbf{J} is given by

$$\mathbf{J} = \mathbf{L} + \mathbf{j} = \mathbf{L}' + \mathbf{j}', \quad (15)$$

with the initial and final orbital angular momentum \mathbf{L} and \mathbf{L}' perpendicular to the initial and final relative velocity vectors \mathbf{v} and \mathbf{v}' , and \mathbf{j} and \mathbf{j}' the rotational angular momenta of reactants and products. Since bulk experiments indicate that the reaction of $\text{C}(^3P_j)$ with CH_3CCH proceeds within orbiting limits⁵⁶ and our relative cross sections rise with decreasing collision energy (Sec. III E), an upper limit of the impact parameter, b_{max} , is determined via the classical capture theory.^{56,57} Approximating the Lennard-Jones coefficient C_6 according to Hirschfelder *et al.*⁵⁸ and using the ionization potentials $E_{\text{C}(^3P_j)} = 11.76 \text{ eV}$, $E_{\text{C}_3\text{H}_4} = 10.36 \text{ eV}$, and polarizabilities $\alpha_{\text{C}(^3P_j)} = 1.76 \times 10^{-30} \text{ m}^3$, $\alpha_{\text{C}_3\text{H}_4} = 6.18 \times 10^{-30} \text{ m}^3$,⁵² b_{max} gives rise to $b_{\text{max}}(20.4 \text{ kJmol}^{-1}) = 3.8 \text{ \AA}$ and $b_{\text{max}}(33.2 \text{ kJmol}^{-1}) = 3.2 \text{ \AA}$. The maximum orbital angular momentum yields $L_{\text{max}}(20.4 \text{ kJmol}^{-1}) = 116\hbar$ and $L_{\text{max}}(33.2 \text{ kJmol}^{-1}) = 125\hbar$. Since CH_3CCH is produced in a supersonic expansion and j peaks at $2-4\hbar$ for typical rotational temperatures between 20 and 40 K, \mathbf{j} contributes less than 2.5% to the total angular momentum \mathbf{J} , and Eq. (15) reduces to

$$\mathbf{L} \approx \mathbf{J} = \mathbf{L}' + \mathbf{j}'. \quad (16)$$

To justify the weak $T(\theta)$ polarization, \mathbf{L} and \mathbf{L}' must be uncoupled with $\mathbf{j}' \gg \mathbf{L}'$, and the initial orbital angular momentum becomes the final rotational angular momentum. This weak $\mathbf{L}-\mathbf{L}'$ correlation is a direct result of the inability of the departing H atom to carry significant orbital angular momentum. On the other hand, a strong $\mathbf{L}-\mathbf{L}'$ correlation would have indicated that the complex decomposed with $\mathbf{L}' \gg \mathbf{j}'$, but the expected $(\sin \theta)^{-1}$ shaped $T(\theta)$ at 20.4 kJmol^{-1} is clearly not observed.

E. Flux contour maps and total relative cross sections

Figures 8 and 9 show center-of-mass flux contour maps $I(\theta, E_T) \sim T(\theta) \times P(E_T)$ for collision energies at 20.4 and 33.2 kJmol^{-1} . Data at lower collision energy depict a forward-backward symmetric flux profile as expected from the center-of-mass angular distribution. With increasing collision energy, the pronounced forward peaking on the relative velocity vector is evident. Integrating this flux distribu-

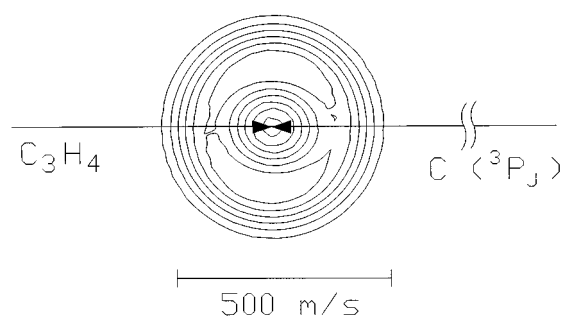


FIG. 8. Contour flux map for the C_4H_3 product from the reaction $\text{C}(^3P_j) + \text{CH}_3\text{CCH}(X^1A_1)$ at a collision energy of 20.4 kJmol^{-1} .

tion and correcting for the reactant flux as well as relative reactant velocity, we find a total, relative cross section ratio of $\sigma(20.4 \text{ kJmol}^{-1})/\sigma(33.2 \text{ kJmol}^{-1}) = 1.7 \pm 0.4$. This finding together with recent bulk experiments⁵⁶ suggest a barrierless, attractive long-range dispersion forces dominating the $\text{C}-\text{CH}_3\text{CCH}$ interaction as well as a loose, reactant-like transition state located at the centrifugal barrier to the triplet C_4H_4 PES at about 3 \AA .

F. Energy partition of total available energy

The identification of the $n\text{-C}_4\text{H}_3$ isomer allows us to estimate partition of the total available energy, E_{tot} into product translation, E_{tr} , $\approx \langle E_T \rangle$. Even if the butatrienyl structure resembles only an inversion transition state, the 3 kJmol^{-1} barrier can be easily overcome at experimental conditions applied here. The quasilinear $n\text{-C}_4\text{H}_3$ radical holds the rotational constants $A = 10.17 \text{ cm}^{-1}$, $B = 0.139 \text{ cm}^{-1}$, and $C = 0.137 \text{ cm}^{-1}$ and classify it as a highly prolate asymmetric top with asymmetry parameter $\kappa = -0.9996$, Fig. 10. Hence, we approximate the rotational levels to those of a rigid symmetric top¹⁷ using the rotational quantum number $J = 116$ ($E_{\text{coll}} = 20.4 \text{ kJmol}^{-1}$) and $J = 125$ ($E_{\text{coll}} = 33.2 \text{ kJmol}^{-1}$) cf. Sec. III D, and calculate the component of the rotational angular momentum about the principal axis K with $K = 0$ for no rotation about the figure axis, but perpendicular to it, and

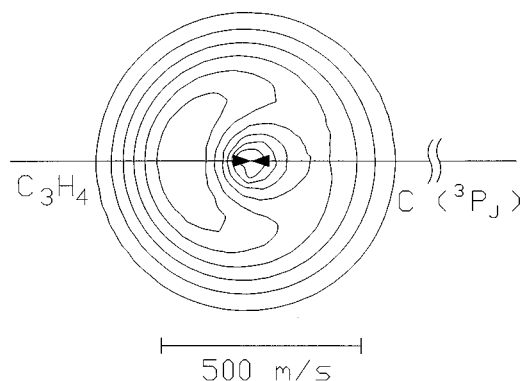


FIG. 9. Contour flux map for the C_4H_3 product from the reaction $\text{C}(^3P_j) + \text{CH}_3\text{CCH}(X^1A_1)$ at a collision energy of 33.2 kJmol^{-1} .

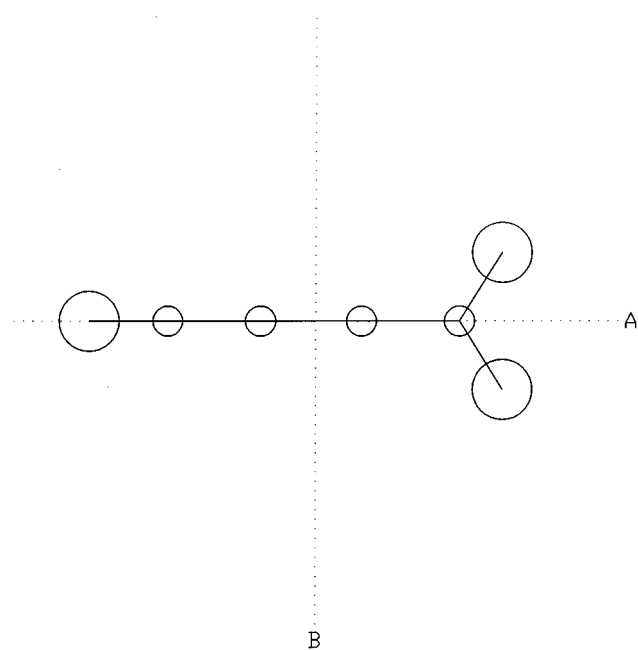


FIG. 10. Principal rotation axis of the butatrienyl radical. The C -axis is perpendicular to the paper plane.

$K \approx J$ for a fast rotation about the principal axis, with a slow end-over-end one. Since no data on the K -distributions are available, we use the same procedure as applied for the $C(^3P_j) + C_2H_4$ system¹⁷ and calculate first the rotational energy assuming $K=0$ ("low K approximation"). This gives us the maximal vibrational energy release E_{vib} in the n - C_4H_3 radical. Hereafter, the highest energetically accessible K states K_{max} are computed assuming $E_{\text{vib}}=0$ kJmol^{-1} to estimate an upper limit of the product rotational excitation as well as an order of magnitude of the lowest tilt angle α_{min} of the n - C_4H_3 principal inertial axis with respect to \mathbf{j}' in terms of the classical vector model.¹⁷

The low K approximation yields a nearly constant partitioning of total energy into rotational degrees of freedom at both collision energies, i.e., 21 ± 2 kJmol^{-1} ($10 \pm 1\%$) vs 26 ± 3 kJmol^{-1} ($11 \pm 2\%$). Further, the fraction of the maximum vibrational energy release stays constant within the error limits ($68 \pm 20\%$ and $59 \pm 10\%$; 145 kJmol^{-1} at lower and 133 kJmol^{-1} at higher collision energy) and might suggest a lifetime long enough to randomize the energy into the vibrational modes of the C_4H_4 complex. Finally, even in the limit of zero vibrational excitation of the n - C_4H_3 product and a maximum K value, the principal axis is tilted 73° – 76° with respect to \mathbf{j}' and clearly demonstrates a predominant end-over-end-rotation of the n - C_4H_3 radical.

IV. DISCUSSION

In this section, we outline feasible reaction pathways on the triplet C_4H_4 PES to produce C_4H_3 isomers (1)–(6) via insertion of the electrophile carbon atoms into the C–H and C–C bonds of methylacetylene, addition to two π -molecular orbitals at both distinct carbon atoms, and, finally, addition

to two π -orbitals at one carbon atom. The observed CM angular and translational energy distributions are then compared to what is expected based on these channels. Pathways incompatible with experimental data are dismissed. Since no C_4H_4 intermediate fulfills requirements for intersystem crossing,¹⁷ the discussion is restricted to the triplet surface. However, neither *ab initio* nor experimental enthalpies of formations of triplet C_4H_4 isomers are available, and their energetics are approximated based on corresponding triplet C_3H_2 isomers.^{59–65}

A. C_4H_4 potential energy surface

Addition of $C(^3P_j)$ to two perpendicular π -orbitals at the methylacetylene α -C atom (the neighboring carbon atom to the methyl group) yields triplet *s-cis/trans* 2-methylpropendiylidene (11)/(12), Fig. 11, whereas attack to the β -C atom forms triplet *s-trans/cis* 1-methylpropendiylidene (13)/(14). Since *trans*-propendiylidene is energetically favored by about 80 kJmol^{-1} as compared to the *cis* isomer on the triplet C_3H_2 surface, this difference is adapted to *cis* (11)/(14) vs *trans* (12)/(13) isomers. Further, we approximate identical enthalpies of formations of (11)/(14) ($\Delta_f H = 815$ kJmol^{-1}) and (12)/(13) ($\Delta_f H = 735$ kJmol^{-1}). (13)/(14) undergo [2,1]-H-migration to triplet 1-methylpropadienylidene (15), [2,3]-H-rearrangement to triplet 1-methylpropargylene (16), ring closure to triplet methylcyclopropenylidene (17), or direct C–H fragmentation to the linear C_4H_3 isomer (5). Two remaining channels are energetically not accessible: H loss of the methyl group yields a 1,3,3-triradical which—if it existed—suffers ring closure to a tri or tetra cycle which is less stable than the already closed channel to (10); the [1,2] methyl group migration to triplet 2-methylpropanediylidyne (19) is endothermic by 150 kJmol^{-1} . Similar to (13)/(14), (11)/(12) might react via [2,3] or [2,1] CH_3 -migration to (16) and (15), respectively. Besides addition to α -C-atom, $C(^3P_j)$ might add to both α - and β -C-atoms of the methylacetylene molecule, generating methylcyclopropenylidene (17).

Furthermore, $C(^3P_j)$ insertion into the acetylenic C–H as well as the C–C single bond might lead to triplet methylpropargylene (16), whereas insertion into the aliphatic C–H bond of the methyl group forms a triplet carbene (20). The fate of (15)–(17) is governed by C–H fragmentation and/or H-migration: (17) decomposes via C–H bond rupture to (4) or (3), then rearranges to triplet methylenecyclopropene (21), which is followed by H-loss to (3) or (6); the only energetically feasible fragmentation of (15) yields C_4H_3 isomer (5), whereas (16) decomposes either to (5) or n - C_4H_3 (1). Finally, (15) might rearrange via hydrogen migration to triplet vinylidene carbene (22).

The reaction pathway to the identified n - C_4H_3 radical (Sec. III C) can only proceed via hydrogen loss from the CH_3 group of triplet 1-methylpropargylene (16). Here, the preference of the methyl H -atom loss compared to the acetylenic C–H bond cleavage even at higher collision energy correlates with the ~ 140 kJmol^{-1} weaker aliphatic carbon-hydrogen bond energy and excludes decomposition of (16) to C_4H_3 isomer (5). Additionally, the identification

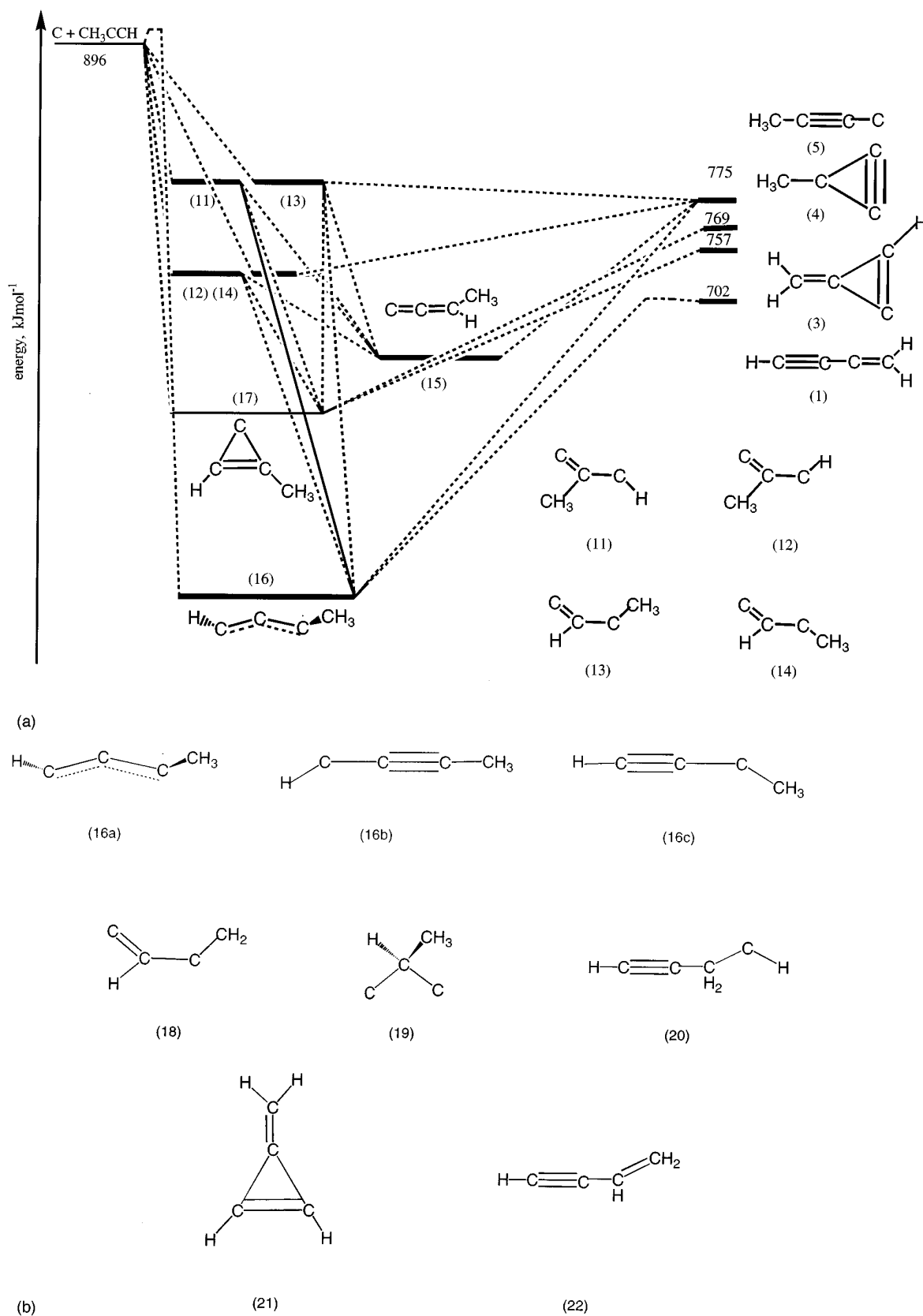


FIG. 11. (a) Schematic representation of the lowest energy pathways on the triplet C_4H_4 PES and structures of potentially involved collision complexes. Triplet methylenecyclopropane and vinylacetylene are not included, since their singlet-triplet gaps have not been investigated yet. (b) Additional structures for possible intermediates and products relevant to the discussion. Three potential electronic structures of propargylene are presented: 1,3-diradical (16a) and carben-like structures (16b/c). Isomers (11)–(14) are named with respect to atoms/groups at the former acetylenic triple bond.

of Eq. (16) as the decomposing complex eliminates the possibility the symmetric $T(\theta)$ originates from a symmetric complex (Sec. III D), since rotation around any principal axis cannot fulfill this requirement. The remaining question to be solved is the reaction pathway to (16). Insertion of $C(^3P_j)$ into the acetylenic C–H bond can be rejected, since only a narrow range of impact parameters between 1.19 and 2.24 Å would contribute to reactive scattering signal. The overwhelming contribution of large impact parameters to the capture process up to 3.8 Å was already mentioned in Sec. III D and III E. Additionally, no evidence of insertion was found in the crossed beam reaction of $C(^3P_j)$ with unsubstituted acetylene⁶⁹ indicating that the symmetry-forbidden insertion into the acetylenic C–H bond involves a barrier of at least 33.2 kJmol⁻¹. Insertion into the C–C single bond can be excluded as well: The forward peaking center of mass angular distribution requires the inserted carbon atom and the leaving hydrogen to be located on opposite sides of the rotation axis of fragmenting (16). However, this condition is not satisfied. In addition, hot atom tracer experiments of $^{11}C(^3P_j)$ with C_2H_6 and even strained cyclobutane rings show a screening of the C–C bond by hydrogen atoms, and only insertion into C–H bonds is observed.⁶⁶ Therefore, any insertion process can be excluded from the discussion.

Remaining pathways to (16) involve triplet C_4H_4 intermediates (11)–(14). Using the concept of regioselectivity of electrophilic radical attacks on substituted olefines and extending it to alkynes,⁶⁷ we can eliminate further collision complexes. The framework predicts the radical attack to be directed at the carbon center which holds the highest spin density. Since partial delocalization of the methyl π -group orbitals increases the spin density on the β -C-atom at the expense of the α -position, $C(^3P_j)$ attacks preferentially at the β -C. Additionally, the sterical hindrance of the CH_3 group reduces the cone of acceptance at the α -C-atom and the range of reactive impact parameters. Both effects together direct the electrophilic carbon addition to (13)/(14). Even if (11) and (12) were formed to a minor extent, rearrangement to (16) would involve a CH_3 -group ($m=15$) migration which is unfavorable compared to rearrangement of the light H atom to (16) via (12)/(13). Similar arguments eliminate a simultaneous attack of $C(^3P_j)$ to α - and β -C-atom with maximum impact parameters of about 0.6 Å to (17). Both prevailing pathways to (16) via (13) and (14) cannot be discriminated based on our experimental data. The chemical dynamics to alternative C_4H_3 isomers at lower collision energy involve isomers (13)–(15), (17), or (20). The last one can be ruled out, since insertion of $C(^3P_j)$ into the aliphatic C–H bond does not play a role. Results of crossed beam experiments $C(^3P_j)+CH_4$ at relative collision energies up to 40 kJmol⁻¹ show no reactive scattering signal of insertion into the aliphatic C–H bond.⁶⁸ Therefore—if (2) contributes—hydrogen loss of triplet vinylacetylene (22) represents the only open channel.

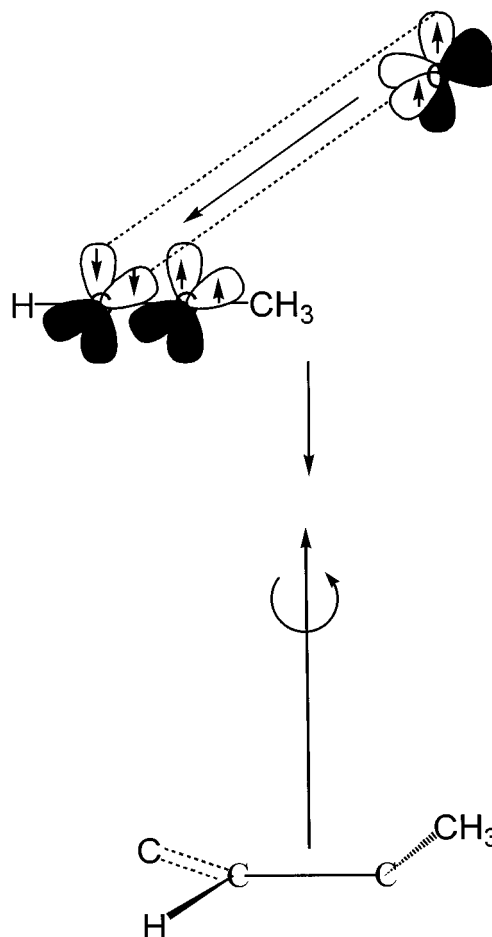


FIG. 12. Approach geometry of the carbon atom toward the methylacetylene molecule conserving C_s symmetry and induced rotation around the B -axis.

B. Rotation axis of the triplet 1-methylpropargylene complex

Conserving the C–C–C–C-plane as a plane of symmetry, the singly occupied p_x and p_z orbitals of the carbon atom might add to the π_x - and π_z -orbitals under C_s symmetry on the $^3A'$ surface to form isomers (13)/(14), Fig. 12. This pathway supports a maximum orbital overlap to the C–C- σ - and C–C- π -bond via interaction of p_x with π_x - as well as p_z with π_z -orbitals. Oblique approach geometries are supported as well and open larger impact parameters for the reaction as discussed in Sec. III E. Since $L \approx j'$, the four carbon atoms rotate in a plane approximately perpendicular to L around the C -axis of the prolate 1-methylpropendiylidene. The consecutive hydrogen shift to 1-methylpropargylene conserves either the symmetry plane [assuming C_s symmetry of (16b) or (16c), Fig. 12] or follows C_1 symmetry (geometry (16a)). Since the adduct still rotates around the C -axis, the added carbon atom in the C_4 position and the methyl hydrogens are located on opposite sites of the rotation axis as required to explain the forward-peaking C_4H_3 product with respect to the carbon beam. This almost in-plane rotation yields extremely low K values as well as a minor J component about the

figure axis of the 1-methylpropargylene and can be related to dominating low K states populated in the n -C₄H₃ product (Sec. III F).

An alternative C(³P_{*j*}) trajectory under C₁ symmetry on the ³A surface might induce rotations about the *A*, *B*, and *C* axes of 1-methylpropendylidene and—after H migration—of 1-methylpropargylene, but does not support a maximum overlap of both perpendicular *p*- with π -orbitals. Furthermore, a freely rotating CH₃ group in (16) undermines *A*-like rotations, since its hydrogen atoms rotate to the same side as the incorporated carbon atom. Hence, the required forward-peaked $T(\theta)$ cannot be supplied.

C. Lifetime of the triplet 1-methylpropargylene complex

The rotational period of the 1-methylpropargylene complex can act as a clock in the molecular beam experiment and can be used to estimate the lifetime τ of the decomposing complex at a relative collision energy of 33.2 kJmol⁻¹. The osculating model relates the intensity ratio of $T(\theta)$ at both poles to τ via Eq. (17)

$$I(180^\circ)/I(0^\circ) = \exp\left(-\frac{t_{\text{rot}}}{2\tau}\right), \quad (17)$$

where t_{rot} represents the rotational period with:

$$t_{\text{rot}} = 2\pi I_i / L_{\text{max}}. \quad (18)$$

I_i represents the moment of inertia of the complex rotating around the *i*-axis, and L_{max} the maximum orbital angular momentum. Using the *ab initio* geometries of propargylene and a C–CH₃ distance in (16) of 1.47 Å, we can estimate the rotational period of the methylpropargylene complex: around the *A* axis we find $t_{\text{rot}}(A) = 0.01$ – 0.02 ps, and around the *B/C* axis we obtain $t_{\text{rot}}(B, C) = 1$ – 2 ps. Plugging in all data in Eq. (17) yields a lifetime of the triplet 1-methylpropargylene complex equal to one rotational period. The absolute value of τ depends dramatically on the rotation axis, i.e., *B*, *C* vs *A*. Since reactions with a collision time $\ll 0.1$ ps follow direct scattering dynamics, the $T(\theta)$ at 33.2 kJmol⁻¹ relative collision energy should be strongly forward peaked, if the complex rotated around the *A*-axis. Our data show only a moderate peaked center-of-mass angular distribution at 33.2 kJmol⁻¹ and an isotropic one at 22.4 kJmol⁻¹. Therefore, rotation about the *A* axis can be eliminated as already suggested in Sec. IV B, and end-over-end rotation around the *B*- or *C*-axis of (16) takes place. Due to the optimal orbital overlap (Sec. IV B), *C*-like rotations should dominate. Compared to the forward peaked $T(\theta)$ as found in the crossed beam reaction C(³P_{*j*}) + C₂H₂ → C₃H + H at a relative collision energy of 8.8 kJmol⁻¹, the enhanced complex lifetime is a direct consequence of the additional 9 vibrational modes of the CH₃ group. A similar behavior contributes to the increased lifetime of the triplet 1-methylallene complex [crossed beam reaction C(³P_{*j*}) + C₃H₆ → C₄H₆ → C₄H₅ + H (Ref. 69)] vs triplet allene [crossed beam reaction C(³P_{*j*}) + C₂H₄ → C₃H₄ → C₃H₃ + H (Ref. 69)].

D. Exit transition state

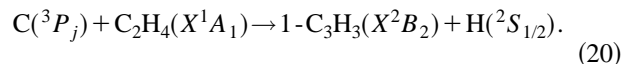
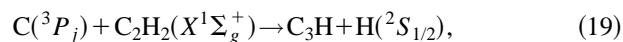
The partitioning of the total available energy into the translational, rotational, and vibrational degrees of freedom of the n -C₄H₃ radical as well as the collision energy dependent $P(E_T)$ shape reveal information on the exit transition state. The framework of an ideal RRKM system requires that exit channel interactions, i.e., the coupling between the reaction coordinate (translation) and internal motion beyond the critical configuration, must be small. This condition is only fulfilled in loose transition states, implying the reverse reaction of H + n -C₄H₃ to 1-methylpropargylene holds no entrance barrier. As shown in Sec. III C, the exit transition state is located at least 30–60 kJmol⁻¹ above the products, indicating that the C–H bond rupture in triplet 1-methylpropargylene does not follow the patterns of an ideal RRKM system with a loose transition state. On the other hand, Marcus' tight transition state theory quantifies a rising fraction of total available energy into vibration with increasing collision energy, if the decomposing triplet C₄H₄ complex has many degrees of freedom. Both $P(E_T)$ s clearly underline a tight transition state, but within our error limits, a complete energy randomization cannot be proved or disproved. These deviations from the loose transition state are based on dynamical effects during the separation of fragments into products together with a significant geometry change from the triplet 1-methylpropargylene complex. Comparing the bond orders (*BO*) of n -C₄H₃, Fig. 1 (1a/b) with those of methylpropargylene, Fig. 11 (16a–c), supports this approach: In the case of a propargylene-like, 1-3 diradical (16a), the C–C bond orders change from two times 2.5 and 1.0 to an acetylenic (*BO* = 3), olefinic (*BO* = 2) and shifted aliphatic C–C bond (*BO* = 1). If (16) exists as a triplet carbene (16b/c), the conversion of the C–C single bond located at the carbene center to a partially delocalized C=C bond increases the bond strength by ~ 250 kJmol⁻¹. Finally, an isotropic $T(\theta)$ distribution as compared to the forward peaked distribution seen in the reaction C(³P_{*j*}) + C₂H₂ → C₃H + H (Sec. III D and Ref. 17) implies the additional modes of the CH₃ group induce the long-lived complex behavior and that the energy randomization in the collision complex might be complete.

E. Alternative isomers at lower collision energy

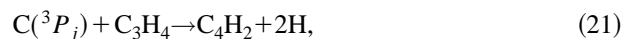
Based on our experimental results, any of the pathways to C₄H₃ isomers (2)–(6) might show additional contributions at lower collision energy. The electron density change of each triplet C₄H₄ complex fragmenting to (3)–(6) suggest a tight transition state as expected from the center of mass translational energy distribution. Since the relative collision energy increases by only 10 kJmol⁻¹, formation of only one isomer of (2)–(6) with no n -C₄H₃ formation is hard to explain. The isotropic center-of-mass angular distribution might open a potential two channel fit of n -C₄H₃ and a second C₄H₃ isomer as well. However, neither transition state frequencies are available, and the experimental data alone cannot resolve this question.

V. IMPLICATIONS TO INTERSTELLAR CHEMISTRY AND COMBUSTION PROCESSES

The crossed beam setup represents a versatile tool to study reaction products as well as chemical dynamics of neutral–neutral reactions relevant to combustion processes and interstellar chemistry under well-defined reactant conditions. Here, the explicit identification of the n -C₄H₃ radical under single collision conditions depicts a third example of the carbon–hydrogen exchange channel in the reaction of C(³P_{*j*}) with unsaturated hydrocarbons studied recently in our lab^{7,17}



This reaction class presents an alternative to ion–molecule reactions to synthesize carbon-chain molecules in the interstellar medium^{7,17} and strictly excludes the formation of any C₄H₂ isomer via



as postulated based on thermochemistry and spin conservation¹⁴ underlining the need of systematic laboratory studies to establish a well-defined data base for neutral–neutral reaction products. A rising cross section with decreasing translation energy underlines the potential contribution of these processes in interstellar clouds and should encourage astronomers to search for hitherto undetected C₄H₃ isomers perhaps among unidentified microwave transitions in the spectrum toward the extended ridge of OMC-1. Since deuterated methylacetylenes (CH₃CCD and CH₂DCCH) were identified in OMC-1 and TMC-1, formation of partially deuterated C₄H₂D is expected to take place as well. Terrestrial based microwave spectra of C₄H₃ radicals could be simply recorded during RF discharges of CH₃CCH/He/CO-mixtures.

Likewise, the identification of the n -C₄H₃ radical under single collision conditions as well as via trapping experiments in oxygen rich hydrocarbon flames²⁶ validates inclusion of hydrocarbon radicals even in oxidative flames. Further investigations of C(³P_{*j*}) reactions with unsaturated hydrocarbons are in progress and will supply a new set of reactions as well as products to be incorporated into combustion models.

VI. CONCLUSIONS

The reaction between ground state carbon atoms, C(³P_{*j*}), and methylacetylene, CH₃CCH, was studied at average collision energies of 20.4 and 33.2 kJmol⁻¹ using the crossed molecular beam technique. The carbon atom attacks the π-orbitals of the CH₃CCH molecule via a loose, reactant like transition state located at the centrifugal barrier. The highest symmetric approach follows C_s symmetry on the ground state ³A'' surface. The initially formed 1-methylpropendylidene complex rotates in a plane almost perpendicular to the total angular momentum vector **J** around its C-axis and undergoes hydrogen migration to

1-methylpropargylene. Within 1–2 ps, the complex decomposes via hydrogen emission to n -C₄H₃. The exit transition state is found to be tight and located at least 30–60 kJmol⁻¹ above the products. The explicit identification of the n -C₄H₃ radical under single collision represents a further example of a carbon–hydrogen exchange in reactions of ground-state carbon atoms with unsaturated hydrocarbons. This channel opens a versatile pathway to synthesize extremely reactive hydrocarbon radicals relevant to combustion processes as well as interstellar chemistry.

Note added in proof. The assignment of the symmetry of the electronic wave function for C_{2v} molecules follows the convention that the molecular plane is defined as the mirror plane, e.g., C₃H₃(X²B₂) instead of C₃H₃(X²B₁).

ACKNOWLEDGMENTS

R.I.K. is indebted the Deutsche Forschungsgemeinschaft for a post-doctoral fellowship. This work was supported by the Director, Office of Energy Research, Office of Basic Energy Sciences, Chemical Sciences Division of the U.S. Department of Energy under Contract No. DE-AC03-76SF00098.

- ¹H. Scheffler and H. Elsässer, *Physics of the Galaxy and Interstellar Matter* (Springer, Berlin, 1988).
- ²C. R. Cowley, *An Introduction to Cosmochemistry* (Cambridge University Press, Cambridge, 1985).
- ³Z. K. Alksne, A. K. Alksnis, and U. K. Dzervitis, *Properties of Galactic Carbon Stars* (Orbit Book, Malabar, 1991).
- ⁴W. Schutte, Ph.D. thesis (University of Leiden).
- ⁵D. Bates, L. Spitzner, *Ap. J.* **113**, 441 (1951).
- ⁶T. J. Millar, C. M. Leung, and E. Herbst, *Astron. Astrophys.* **183**, 109 (1987).
- ⁷R. I. Kaiser, Y. T. Lee, and A. G. Suits, *J. Chem. Phys.* **103**, 10395 (1995).
- ⁸K. Roessler, H. J. Jung, and B. Nebeling, *Adv. Space. Res.* **4**, 83 (1984).
- ⁹K. Roessler, *Rad. Eff.* **99**, 21 (1986).
- ¹⁰E. Herbst and C. M. Leung, *Ap. J.* **233**, 170 (1990).
- ¹¹M. M. Graff, *Ap. J.* **339**, 239 (1989).
- ¹²D. C. Clary, T. S. Stoecklin, and A. G. Wickham, *J. Chem. Soc. Far. Trans.* **89**, 2185 (1993).
- ¹³D. C. Clary, N. Haider, D. Husain, and M. Kabir, *Ap. J.* **422**, 416 (1994).
- ¹⁴R. P. A. Bettens, H. H. Lee, and E. Herbst, *Ap. J.* **443**, 664 (1995).
- ¹⁵R. P. A. Bettens and E. Herbst, *E. Int. J. Mass Spectr. Ion. Proc.* **149**, 321 (1995).
- ¹⁶E. Herbst, Lee, D. A. Howe, and T. J. Millar, *Month. Notice. R. Astron. Soc.* **268**, 335 (1994).
- ¹⁷R. I. Kaiser, Y. T. Lee, and A. G. Suits, *J. Chem. Phys.* **105**, 8705 (1996), preceding paper.
- ¹⁸E. C. Sutton, R. Peng, W. C. Danchi, P. A. Jaminet, G. Sandell, and A. P. G. Russel, *Ap. J. Supl. Series* **97**, 455 (1995).
- ¹⁹F. Combes, G. Wlodarczak, P. Encrenaz, and C. Laurent, *Astron. Astrophys.* **253**, L29 (1992).
- ²⁰A. Coustenis, B. Bezdard, D. Gautier, A. MArten, and R. Samuelson, *Icarus* **89**, 152 (1989).
- ²¹C. R. Wu, T. S. Chien, G. S. Liu, D. L. Judge, and J. J. Caldwell, *J. Chem. Phys.* **91**, 272 (1991).
- ²²R. Hannel *et al.*, *Science* **212**, 192 (1981).
- ²³G. R. Gladstone, M. Allen, and Y. L. Yung, *Icarus* **119**, 1 (1996).
- ²⁴D. Toubanc, J. P. Parisot, J. Brillet, D. Gautier, F. Raulin, and C. P. McKay, *Icarus* **113**, 2 (1995).
- ²⁵R. I. Kaiser and K. Roessler, *Ap. J.* (in press).
- ²⁶M. Hausmann and K. H. Homann, *Ber. Buns. Phys. Chem.* **94**, 1308 (1990).
- ²⁷H. Wang and M. Frenklach, *J. Phys. Chem.* **98**, 11465 (1994).
- ²⁸S. P. Walsh, *J. Chem. Phys.* **103**, 8544 (1995).

- ²⁹ J. A. Miller and C. F. Melius, *Comb. Flame* **91**, 21 (1992).
- ³⁰ R. P. Duran, V. T. Amorrbieta, and A. J. Colussi, *J. Phys. Chem.* **92**, 636 (1988).
- ³¹ R. P. Duran, V. T. Amorrbieta, and A. J. Colussi, *Int. J. Chem. Kinetics* **21**, 947 (1989).
- ³² D. J. LeRoy and E. W. R. Steacie, *J. Chem. Phys.* **12**, 117 (1944).
- ³³ M. Frenklach, S. Skokov, and B. Weiner, *Nature* **372**, 535 (1994).
- ³⁴ M. B. Colket, Presented at the 21st Symposium on Combustion, Munich, 1986.
- ³⁵ Y. Hidaka, K. Tanaka, and M. Suga, *Chem. Phys. Lett.* **130**, 190 (1986).
- ³⁶ W. C. Hung, M. L. Huang, Y. C. Lee, and Y. P. Lee, *J. Chem. Phys.* **103**, 9941 (1995).
- ³⁷ S. J. Harris, H. S. Shin, and D. G. Goodwin, *Appl. Phys. Lett.* **66**, 891 (1995).
- ³⁸ T. K. Ha and E. Gey, *J. Mol. Structure* **306**, 197 (1994).
- ³⁹ E. Gey, S. Wiegatz, W. Huehnel, B. Ondruschka, W. Saffert, and G. Zimmermann, *J. Mol. Structure* **184**, 69 (1989).
- ⁴⁰ P. H. Kasai, L. Skattebol, and E. B. Whipple, *J. Am. Chem. Soc.* **90**, 4509 (1968).
- ⁴¹ P. H. Kasai, *J. Am. Chem. Soc.* **94**, 5950 (1972).
- ⁴² A. L. Cooksy, *J. Am. Chem. Soc.* **117**, 1098 (1995).
- ⁴³ W. Weng, T. Bartik, M. T. Johnson, A. M. Arif, and J. A. Gladysz, *Organometallics* **14**, 889 (1995).
- ⁴⁴ A. J. Arce, R. Machado, C. Rivas, Y. DeSanctis, and J. Deeming, *J. Organomet. Chem.* **419**, 63 (1991).
- ⁴⁵ Y. T. Lee, J. D. McDonald, P. R. LeBreton, and D. R. Herschbach, *Rev. Sci. Instr.* **40**, 1402 (1969).
- ⁴⁶ R. I. Kaiser and A. G. Suits, *Rev. Sci. Instr.* **66**, 5405 (1995).
- ⁴⁷ G. O. Brink, *Rev. Sci. Instr.* **37**, 857 (1966).
- ⁴⁸ N. R. Daly, *Rev. Sci. Instr.* **31**, 264 (1960).
- ⁴⁹ J. M. Parson, K. Shobatake, Y. T. Lee, and S. A. Rice, *J. Chem. Phys.* **59**, 1402 (1973).
- ⁵⁰ M. S. Weis, Ph.D. thesis, University of California, Berkeley, 1986.
- ⁵¹ M. Vernon, LBL-Report 12422 (1981).
- ⁵² *Handbook of Chemistry and Physics* (CRC, Boca Raton, 1995).
- ⁵³ S. Walsh, NASA Ames Research Center, Moffet Field (private communication).
- ⁵⁴ W. B. Miller, S. A. Safron, and D. R. Herschbach, *Discuss. Faraday. Soc.* **44**, 108, 291 (1967).
- ⁵⁵ W. B. Miller, Ph.D. thesis, Harvard, Cambridge, 1969.
- ⁵⁶ D. C. Clary, N. Haider, D. Husain, and M. Kabir, *Ap. J.* **422**, 416 (1994).
- ⁵⁷ R. D. Levine and R. B. Bernstein, *Molecular Reaction Dynamics and Chemical Reactivity* (Oxford University Press, Oxford, 1987).
- ⁵⁸ J. O. Hirschfelder, C. F. Curtiss, and R. B. Bird, *Molecular Theory of Gases and Liquids* (Wiley, New York, 1954).
- ⁵⁹ J. M. Bofill, J. Farras, S. Olivella, A. Sole, and J. Vilarrasa, *J. Am. Chem. Soc.* **110**, 1694 (1988).
- ⁶⁰ G. Maier, H. P. Reisenauer, W. Schwab, P. Carsky, V. Spirsko, B. A. Hess, and L. J. Schaad, *J. Chem. Phys.* **91**, 4763 (1989).
- ⁶¹ T. J. Lee, A. Bunge, and H. F. Schaefer, *J. Am. Chem. Soc.* **107**, 137 (1985).
- ⁶² V. Jonas, M. Böhme, and G. Frenking, *J. Phys. Chem.* **96**, 1640 (1992).
- ⁶³ H. Clauberg, D. W. Minsek, and P. Chen, *J. Am. Chem. Soc.* **114**, 99 (1992).
- ⁶⁴ R. Herges and A. Mebel, *J. Am. Chem. Soc.* **116**, 8229 (1994).
- ⁶⁵ W. J. Hehre, J. A. Pople, W. A. Lathan, L. Radom, E. Wasserman, and Z. R. Wasserman, *J. Am. Chem. Soc.* **98**, 4378 (1976).
- ⁶⁶ M. Marshall, Ph.D. thesis, Yale University, 1969.
- ⁶⁷ S. S. Shaik, and E. Canadell, *J. Am. Chem. Soc.* **112**, 1446 (1990).
- ⁶⁸ R. I. Kaiser, Y. T. Lee, and A. G. Suits (unpublished).
- ⁶⁹ R. I. Kaiser, D. Stranges, Y. T. Lee, and A. G. Suits, *J. Chem. Phys.* (to be published).